A mechanically coupled spring compliant Analysis to out-of-plane oscillation

Eng. Jamal Mohammed[1], Eng. Majed Alshammari[2]

1

2.

****Corresponding Contact**

ABSTRACT

This paper proposes a design that uses a symmetrical arrangement of serpentine springs to create a circular plate that can bend out of its plane. The spring system is made up of individual springs that are coupled together in a single plane. In this study, three models to determine the spring system stiffness have been developed, using the serpentine spring, Sigitta, flexural beam theories, and models of equivalent mechanical springs. The results calculated theoretically match those obtained using numerical techniques such as the Finite-Element-Method (FEM), with a margin of error lower than 10% in the suitable spring's size range. Additionally, the proposed spring structure incorporating mechanical coupling proves to be better at reducing mode coupling compared to spring structures that do not have any mechanical coupling.

Keywords; Serpentine Springs, Finite-Element-Method, single plane ,Sigitta ,flexural beam theory, mechanical coupling

INTRODUCTION

A mechanical spring can be defined as a flexible device that is utilised in storing mechanical energy. It is typically made from a material that is able to withstand significant deformation, such as steel or alloy wires. These springs are essential parts in several applications. For example, in MEMS (Micro-Electro-Mechanical Systems) technology, mechanical springs leverage their ability to store and release energy (Guo, et al., 2022). Figure 1 illustrates an example of the main components of MEMS devices.

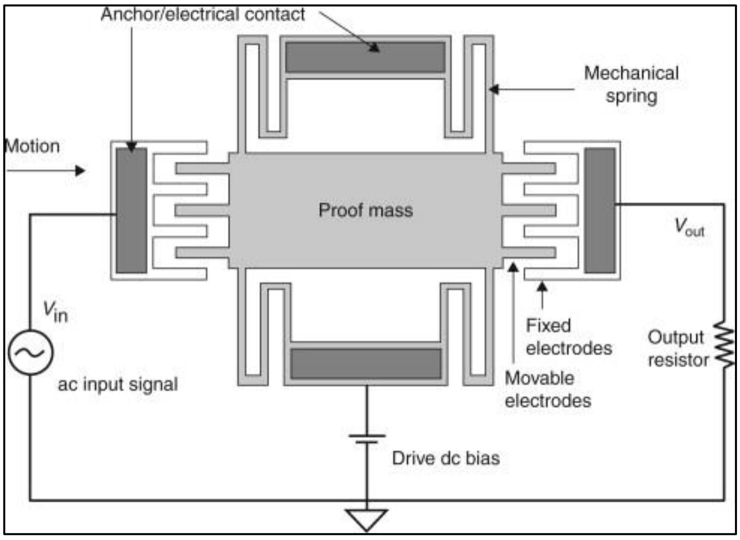

Figure 1: An example of a MEMS device (Guo, et al., 2022)

One everyday use of mechanical springs in MEMS is as a part of micro-scale actuators, which convert electrical energy into mechanical motion on a small scale. These actuators often use electrostatic forces to compress or extend a spring, causing it to move (Larkin, 2020).

Another essential use of springs in MEMS devices is as a part of micro-scale sensors, which detect physical quantities such as acceleration, force, or pressure. These sensors often use the deflection of a spring to translate a physical input into an electrical output (Mouro, et al., 2020). Springs are also used in MEMS oscillators, which are time-keeping devices that utilize the harmonic motion of a spring-mass system. The resonant frequency of these spring-mass systems can be precisely controlled by adjusting the properties of the spring and the mass, allowing them to be used as highly stable timing references in electronic systems (Muscat, et al., 2022).

In MEMS technology, mechanical springs are engineered for specific types of movement, such as single-axis or multi-axis motion, as shown in Figure 2. Various types of springs have been developed to control in-plane motions in these devices. The mechanical springs can be customized to comply with linear movements in the x or y-axis (Zang, et al., 2019).

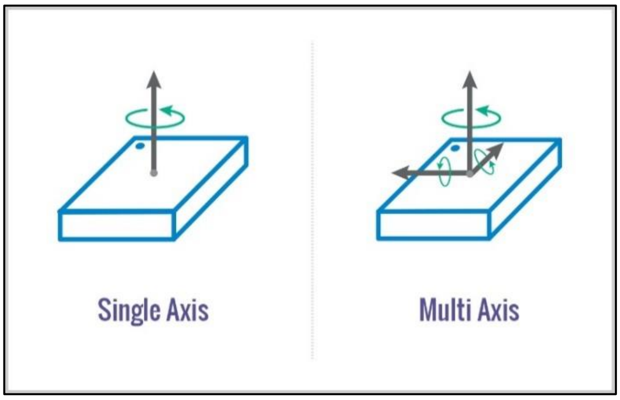

Figure 2: Types of motion (Mouro, et al. 2020)

In the design of these devices, the springs typically consist of straight beams. Some designs incorporate serpentine beams, allowing more significant movement in the x and y axes. Both straight and serpentine beams have also been used for rotational motion (Calmé, et al., 2022). Typically, the individual spring components are separate from one another, with one end linked with a proof mass or structure and the other end fixed to the substrate. Straight beam springs are commonly employed for motion in the out-of-plane z-axis, but their displacement range is limited (Rao, et al., 2019).

To increase the range of motion for micro-actuators' out-of-plane movement, and keep the device size small, both spiral springs and serpentine beams have been developed. When designing micro-actuators, it is essential to carefully select the stiffness of the suspending springs to achieve the desired operational frequency range and actuation voltage. The sensitivity of mechanical sensors is dependent on the stiffness of the suspending springs. The dissimilar devices have various requirements for the operational frequency range.

Inertial switches require a quick response time, typically on the order of microseconds, which translates to operational frequencies in the hundreds of kilohertz. Furthermore, the range of operational frequency for the MEMS accelerometers is between 0.1 Hz and 104 Hz, and they can be used for several applications, including inertial navigation, as well as monitoring explosions (Hu, et al., 2021). Different theories, such as the elastic straight beam theory, the Sigitta spring theory, and the serpentine spring theory, have been used for assessing the suspending spring's stiffness. Recently, a new actuator design that permits out-of-plane movement has been suggested and analysed using the FEM (Buśkiewicz, 2022).

Furthermore, by using a spring design that consists of straight beams surrounding the square plate and connected, it is possible to expand the operational frequency range while reducing the influence of unwanted oscillation modes on the operation.

Despite some advancements, there is still limited research on the use of coupled curve springs, as well as the related theoretical models necessary to evaluate these systems' stiffness, particularly for the low-noise mechanical sensors and low-mode cross-talk micro-actuators purposes. This study introduces a new spring system design that is organized surrounding a circular plate and is acquiescent to the out-of-plane z-axis fluctuations.

In this study, we utilize a design that employs individual serpentine beam springs that are connected to one another in order to decrease unwanted oscillation modes though still allowing for compliance in the z-axis oscillation. The spring design performance is evaluated using the FEM, which will be compared with several similar structures of spring that do not have mechanical coupling. Additionally, we develop theoretical mechanical models to calculate the spring system stiffness and compare the results obtained from these models to the FEM numerical solutions.

SPRING MODEL COMPLIANT TO OUT-OF-PLANE Z-AXIS OSCILLATION

Six serpentine springs are composed of a coupled spring, which is arranged symmetrically around a certain plate to form a circular system (spring system), as represented in Figure 3. Several serpentine springs will be connected at meandering circular/beam arcs. For clarification, this type is known as Type A. In Figure 3 part (a) and Figure 3 part (b), the characteristics of Type A are depicted. The measurements of the width and thickness of the circular arcs in the spring are clarified in Figure 3. In addition to the distance between the arcs of the serpentine spring, which is known as the length of the beam interconnecting in serpentine spring. Additionally, the figures show the gap between the spring arcs, as well as the radius of the centre plate is also represented in the figures and is equal to 50 µm.

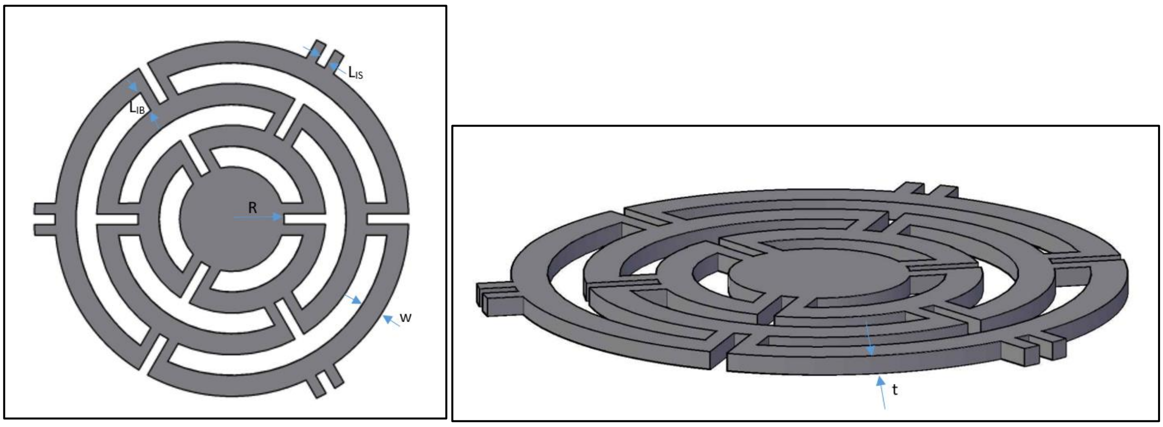

Figure 3: Suggested coupling spring in curved beams in addition to design parameters.

The effect of spring behaviour coupling is investigated based on making a comparison between two similar springs which do not have coupling between the springs circular as clarified in Figure 4. Figure 4 part (a) represents a spring similar what is represented before. Nevertheless, Type B involves removing the connections of the spring circular arc. Figure 4 part (b) is similar to Figure 4 part (a). Another case, the serpentine springs are not axial symmetry, in addition, this case owns a rotational symmetry, which is known with Type C. Type B and Type C are used previously in several studies which are (Dimian & Bildea, 2014) (Hu, et al., 2012) (Wai-Chi, et al., 2010).

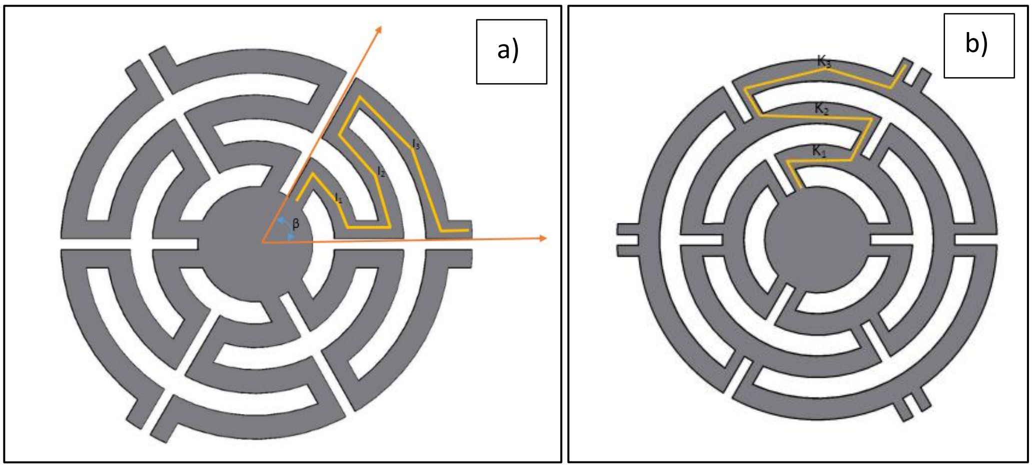

Figure 4: Axial symmetry spring system where (a) rotational symmetry and (b) six-serpentine springs involved in the arcs of circular spring.

Additionally, the range of frequencies that a MEMS device can operate at varies depending on the application (Tu, et al., 2019) (Liu, et al., 2022) and (Jangra, et al., 2021). The frequency at which a MEMS device operates is determined by the dimensions of its spring. While these dimensions can be adjusted or the length of the spring can be increased through adding further stages, the spring couplings' ability in suppressing mode coupling is maintained when compared to similar spring systems without coupling. For this reason, this study utilizes a three stages-spring system as illustrated in Figure 3 and Figure 4.

THE STIFFNESS OF SPRING SYSTEMS CALCULATION

A. An approximate method of straight beams connected in series

This model is made up of multiple elements connected in both series and parallel. The ability of the coupling spring to resist deformation is calculated using this representation, as it determines its stiffness.

$$K_t = 6 \times K_b \qquad (1)$$

In this context, the term Kb refers to the single serpentine spring stiffness, which is multiplied by 6 that indicates the number of serpentine springs. Per the current design, all serpentine springs are composed of 3-circular arc segments. Therefore, the stiffness of Kb is calculated using the current design by Equation (4).

$$\frac{1}{K_b} = \sum_{i=1}^{n} \frac{1}{K_i} \qquad (2)$$

The term K_i represents the ith stiffness for a circular arc spring, and the term n denotes a serpentine spring that comprises (n) circular arc segments. It is possible to approximate the ith circular arc as a straight beam with an effective length of (l_i). The ability of this ith straight beam spring to resist deformation is represented by its stiffness, which can be determined using this Equation (Hibbeler, 1994).

$$K_i = \frac{3EI}{{l_i}^3} \qquad (3)$$

This Equation is often used in the field of mechanical engineering to approximate the circular arc spring's stiffness as a straight beam spring. The Equation relates the stiffness of the ith straight beam spring (K_i) to its moment of inertia (I) and Young's modulus of the spring material (E), as well as the effective length of the ith spring (l_i).

In Equation (3), the straight beam spring' moment of inertia is represented by the variable (I), which is calculated as the product of the width of the spring (w) and the cube of the thickness of the spring (t) divided by 3, $I = wt^3$. The variable (E) represents the spring material's Young's modulus, which is a measure of its stiffness. In the case of a spring made from silicon, the value of (E) would be equal to 1.69 x 10^{11} Newton's per meter. The frequency at which the coupling spring oscillates when not under any external force, known as the natural frequency, is determined by certain factors.

$$f = \frac{1}{2\pi}\sqrt{\frac{K_t}{m}} \qquad \text{Equation (4)}$$

In this context, the variable m represents the total mass of the suspension system, which includes both the serpentine spring beams, as well as the central plate. The value of (m) is determined by using Equation (5).

$$\mathrm{m} = \mathrm{m_{plate}} + \frac{13}{35}\,\mathrm{m_{beam}} \qquad \text{Equation (5)}$$

The formula mentioned here is used to determine the total mass of the suspension system. The variable m_{plate} represents the mass of the central plate and the variable m_{beam} represents the total mass of all the serpentine spring beams. These two values are used to calculate the overall mass of the suspension system; the following two formulas are used to calculate m_{plate} and m_{beam}.

$$m_{plate} = \rho V_{plate} = \rho \pi R^2 t \qquad \text{Equation (6)}$$

$$m_{beam} = 6\rho \sum_{i=1}^{6} V_{beam-i} = \rho \pi R^2 t \qquad \text{Equation (7)}$$

The variable V_{beam-i} represents the volume of the ith beam, which is calculated by multiplying the beam length (l_i), the beam width (w) and the thickness of the beam (t). Both the width and the thickness of the beams are the same for the two designs, but the beam length is different. The variable (ρ) represents the material density. The circular arc spring length is determined using Equation (8).

$$l_i = r_i \beta \qquad \text{Equation (8)}$$

The variable (r_i) represents the radius of the ith spring arc. The radius is calculated by adding the value of R, which is a constant, to the product of i (the index of the spring arc), the sum of the inner beam length (LIB) and the spring width (w). In this study, the angle between the centre of the arc and the tangent of the arc is assumed to be 60 degrees, represented by the variable beta (β).

B. Equivalent Sigitta spring system method

The Equivalent Sigitta spring system is an approach for modelling and studying the performance of mechanical springs. This approach utilizes a representation of Sigitta springs, smaller unit springs. These springs are combined in a specific configuration, either parallel or series. Accordingly, the overall spring is depicted. Spring stiffness and other structural parameters are used to compute the behaviour of the spring.

In this approach, a representation of an equivalent spring is presented in Figure 5, which is comprised of three parts, Figure 5 part (a), Figure 5 part (b), and Figure 5 part (c). Figure 5 part (a) depicts the individual components of the spring, known as unit Sigitta springs. Figure 4 part (b) illustrates how these unit springs are linked in a series configuration. Lastly, Figure 5 part (c) represents the overall shape of the spring, known as a Sigitta-shaped spring, and the parameters used to calculate its stiffness.

In the current research, the mechanical structure comprises three component springs, as represented in Figure 5 part (b), in which these components are in a parallel configuration.

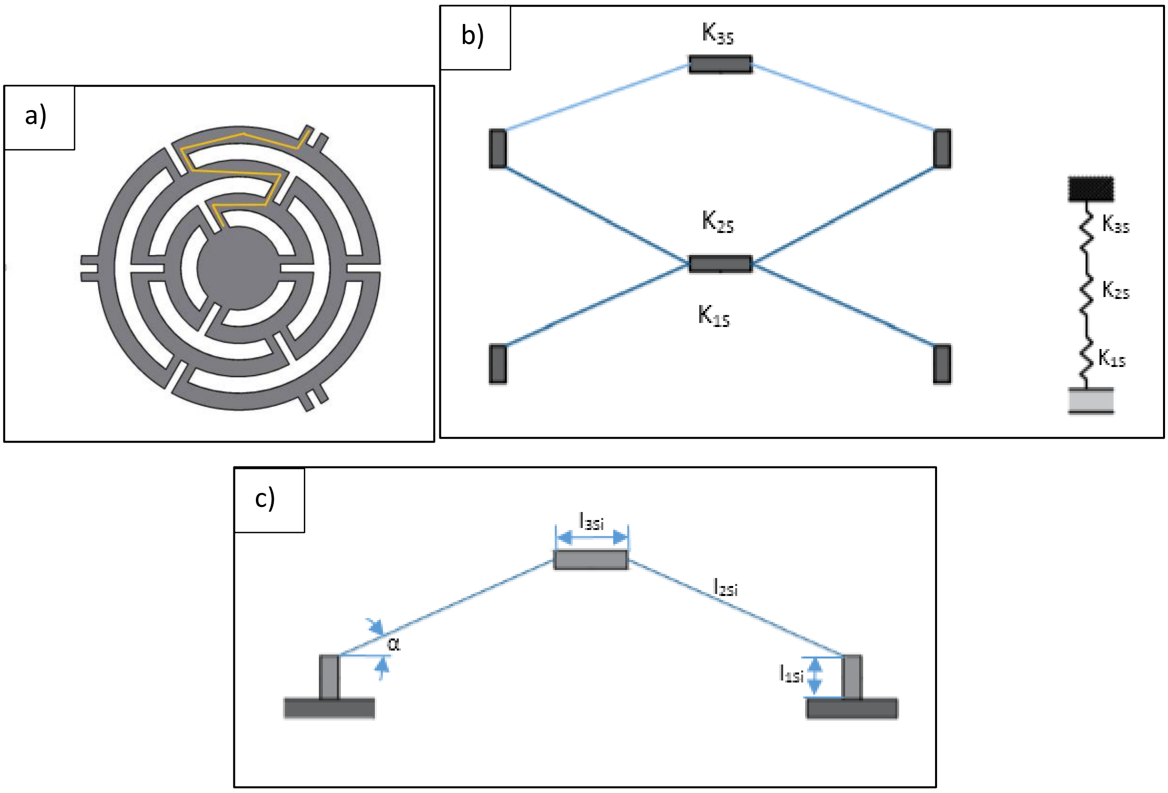

Figure 5: An equivalent Sigitta spring system represented as a coupled spring that breaks it down into individual spring components connected in series.

Thus, the overall stiffness of the spring is determined by combining the stiffness of the three component springs in parallel is represented as follows:

$$K_{ts} = 3 \times K_{3sss} \qquad \text{Equation (9)}$$

Noting that, the spring's total stiffness represented in Figure 4b (K_{3sss}) is determined by Equation (10).

$$\frac{1}{K_{3sss}} = \frac{1}{K_{1s}} + \frac{1}{K_{2s}} + \frac{1}{K_{3s}} \qquad \text{Equation (10)}$$

The stiffness of each Sigitta spring (k_{IS}) is calculated as follows, noting that:

i: 1, 2, or 3.

G: shear modulus, which equals $\frac{E}{2(1+v)}$.

v: Poisson's ratio.

l_{1si}: the connecting beam's length.

l_{2si}: the circular arc spring.

l_{3si}: the length, which equals $w + L_{IS}$.

I_y: the y-axis moment of inertia, which equals $\frac{w\times t^3}{12}$.

I_y: the z-axis moment of inertia, which equals $\frac{w\times t^3}{3}$.

α: 30^o.

Accordingly, the stiffness of each Sigitta spring (k_{IS}) is given by Equation (11):

$$\begin{aligned} k_{IS} = 12\{[6(l_{3si} - 2c_i)^2 sin^2\alpha \\ + 2(l_{1si} + 2l_{3si}\sin\alpha)[l_{1si}\cos\alpha \\ + (2l_{1si}\cos\alpha + l_{3si} - 2c_i)\sin\alpha]\cos\alpha]/(G\ I_t) + [6{l_{1si}}^2 + 14{l_{2si}}^2 \\ + 3(l_{3si} - 2c_i)^2 + 3\left[(l_{3si} - 2c_i)^2 - 2\left({l_{1si}}^2 + {l_{2si}}^2\right)\right]\cos 2\alpha \\ - 6(2c_i - l_{3si})(l_{2si} - 2l_{1si}\sin\alpha)\cos\alpha + 6l_{2si}[(l_{3si} - 2c_i)\cos 3\alpha \\ + l_{2si}\cos 4\alpha + 4l_{1si}\ sin\alpha - 2l_{1si} sin3\alpha]]/(EI_y)\}^{-1}/l_{2si} \end{aligned}$$ Equation (11)

Furthermore, the c_i parameter is computed as presented in Equation (12).

$$c_i = \frac{\begin{Bmatrix} GI_t[l_{3si}\cos\alpha + l_{2si}\cos 2\alpha]\cos\alpha \\ +\left(EI_y - GI_t\right) l_{1si}\sin\alpha\cos\alpha + EI_y(l_{3si} + 2l_{2si}\cos\alpha)sin^2\alpha \end{Bmatrix}}{2(G\ I_t\ cos^2\alpha + EI_y\ sin^2\alpha)}$$ Equation (12)

C. The equivalent serpentine spring system

This system is an approach for spring representation by using multiple identical serpentine springs linked in parallel. Thus, the total spring stiffness is computed by multiplying the stiffness value of each individual spring component by the number of serpentine springs used in the system. This approach involves the study of the overall spring as comprised of six similar springs connected in a parallel configuration. Figure 2 represents the single serpentine spring, and l_i considered below is the length of the ith arcs. The total stiffness of the spring (K_{ts}) is computed by multiplying the stiffness of each individual spring by six, in which the stiffness of every individual serpentine spring is known as (K_{zs}) and represented in Equation (13). Knowing that the h parameter is determined by Equation (14).

$$K_{zs} = \frac{1}{\left\{\sum_{n=1}^{3}(60n)\times\left(\sqrt{\frac{nw\sqrt{L_{IB}}}{l_n t}}\right)\times\left(\frac{{l_n}^2}{Gh}\right)\times\left(\frac{Gh}{EI_y}l_n + 3\ L_{IB}\right)\right\}}$$ Equation (13)

$$h = t\ w^3\left\{0.333 - 0.21\frac{w}{t}\left(1 - \frac{w^4}{12\ t^4}\right)\right\}$$ Equation (14)

RESULTS AND DISCUSSION

The study presents the results of simulating the behaviour of spring systems in various operating modes. The mechanical connection between the out-of-plane oscillation mode at z-axis and the closest oscillation mode is evaluated based on these simulations.

A. Results

The simulation uses spring parameters of $R = 50\ \mu m$, $w = 20\ \mu m$, $t = 10\ \mu m$, $L_{IS} = 10\ \mu m$ and $L_{IB} = 20\ \mu m$. To examine the impact of mechanical coupling, the frequency variation among the operating mode (mode z) and the second mode (mode 2) is considered.

$$\delta_f = ((f_{Mode2} - f_{ModeZ})/f_{ModeZ}) * 100\% \qquad \text{Equation (15)}$$

The percentage of coupling between different operating modes in the system is type A ($\delta_{f\text{-type A}}$) is 60.8%, type B ($\delta_{f\text{-type B}}$) is 52.8%, and type C ($\delta_{f\text{-type C}}$) is 53.1%. This ensures that there is mechanical isolation between the operating mode and neighbouring modes.
of-plane oscillation mode at z-axis, and (d) to (f) are the second modes. The system parameters for the spring are specified as R = 50 µm, w = 20 µm, t = 10 µm, L_{IS} = 10 µm, as well as L_{IB} = 20 µm.
To evaluate the performance of three different spring types, the effect of mode coupling will be examined by analysing the relationship between δ_f and the representative dimensions of the spring. Specifically, we will vary the width w of the spring between 2 µm and 20 µm besides keeping the other parameters fixed. The results of this investigation are presented in Figure 6 and Figure 7. Figure 6 part (a) and Figure 6 part (b) displaying the frequencies of mode z and mode 2, while Figure 7 part (a) and Figure 7 part (b) displaying the mode z and δ_f stiffness for each of the studied spring types.

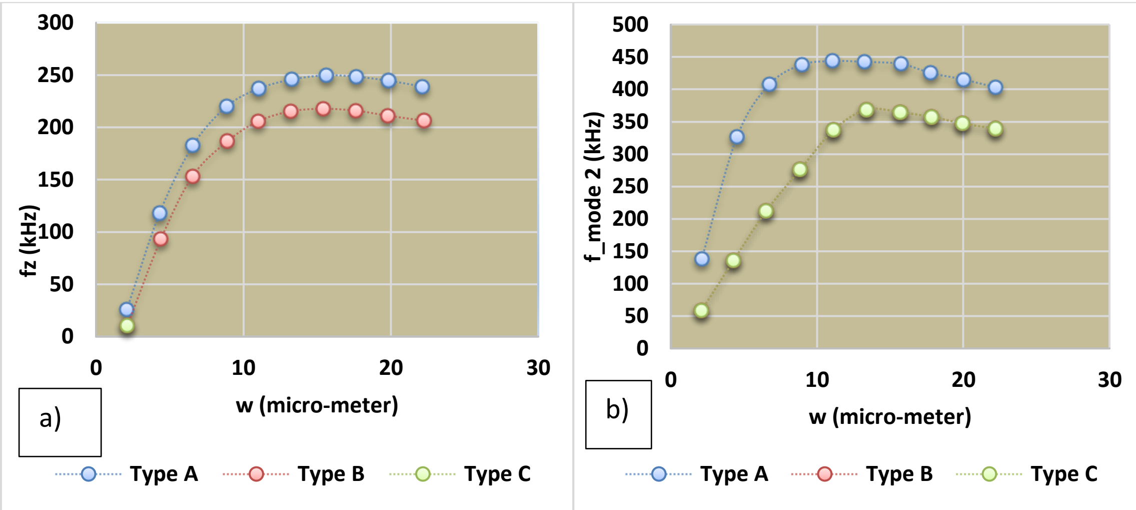

Figure 6: (a) z-mode frequency, (b) mode 2 frequency.

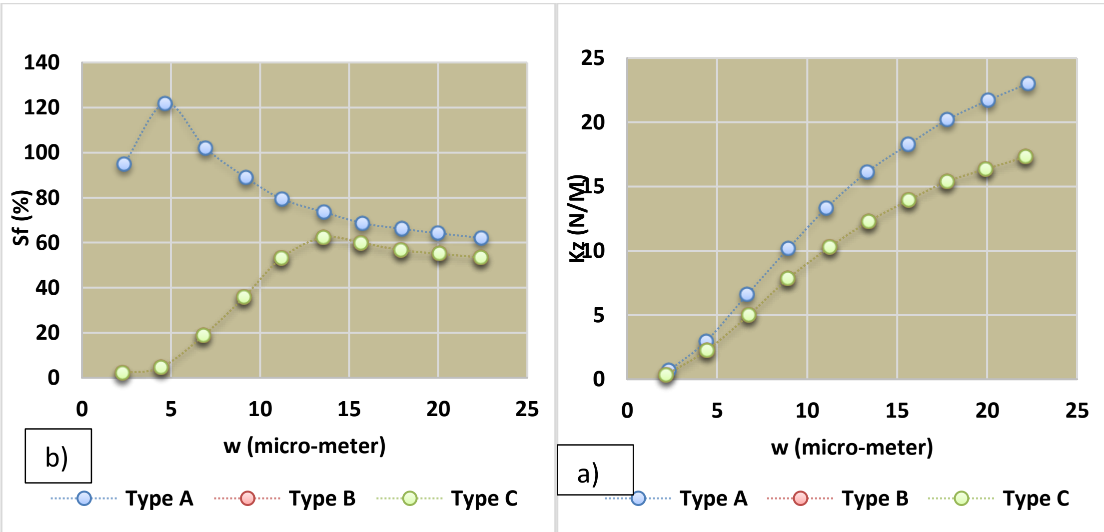

Figure 7: (a) z-mode stiffness (b) δ_f for the three types of the proposed springs as a function of w.

Accordingly, the set frequencies for the distinct three types of spring could be altered from 70000 Hz to 260000 Hz for the first type, "Type A", while for the second and third types "Type B and Type C", the frequencies can be altered from 55000 Hz to 220000 Hz. For mode z, the frequency characteristic starts increasing till reaching the maximum. Then, it then starts to be decreased gradually when the circular arc width increases. The outcomes showed that both of Type C and Type B have the same δ_f and frequencies. Particularly, when the arc of the circular spring increases, the corresponding δ_f of Type A will decrease with a percentage greater than 60%.

In this investigation, the thickness of the circular arc spring, represented by (t), ranges between (2 and 20) μm while other parameters were fixed, as represented in Figure 5. Furthermore, the results obtained are shown in Figure 8 and Figure 9.

Additionally, it was found that the z-mode and mode 2 operating frequencies, besides the frequency difference (δ_f) for type B and type C, remained the same within the investigated range of t. However, for type A, δ_f increased linearly from 75% to 90% with increasing the t value from (2 to 20) μm. On the other hand, for type B and type C, δ_f decreases from around 65% to 5% for the same t values.

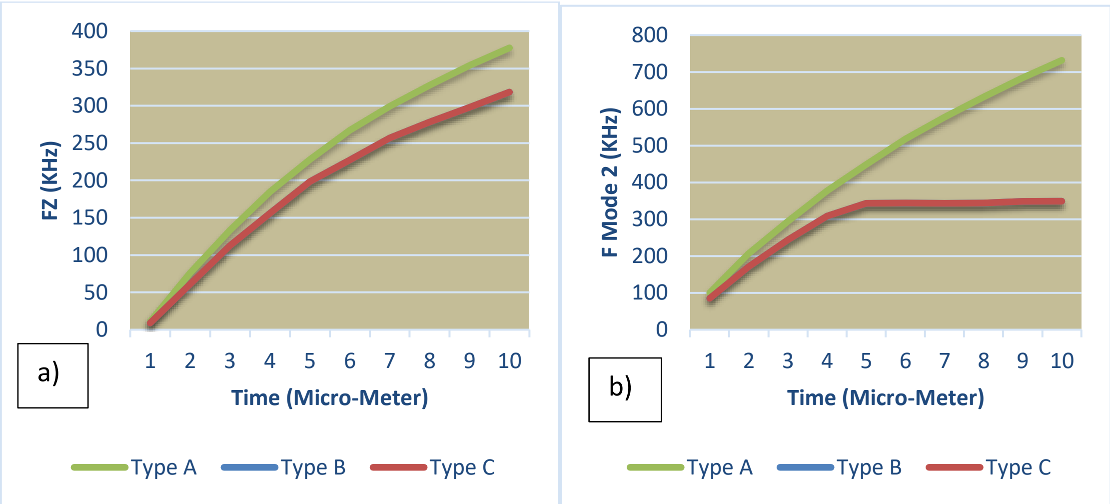

Figure 8: (a) z-mode frequency, (b) mode 2 frequency.

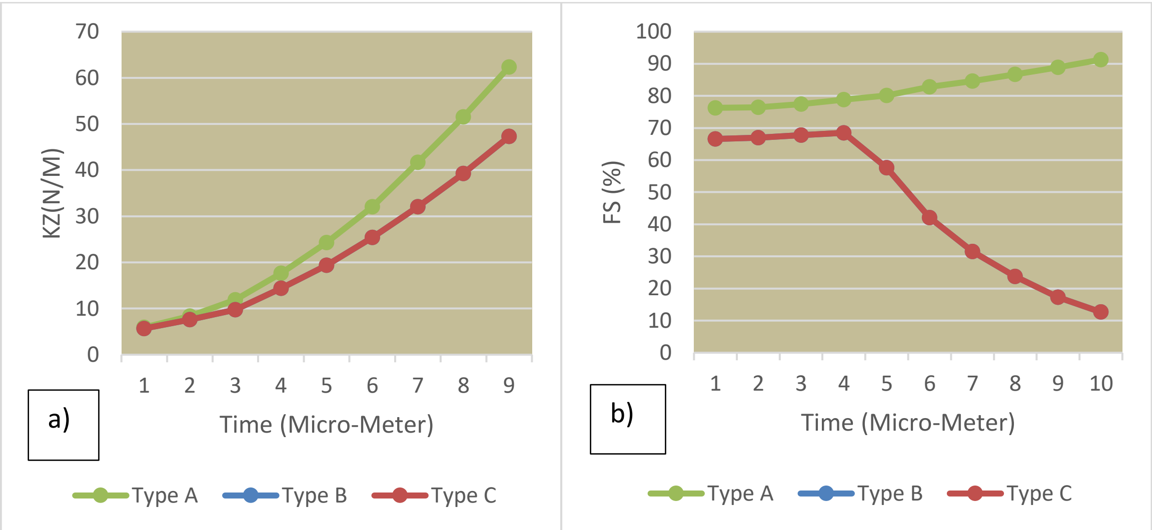

Figure 9: (a) z-mode stiffness (b) δ_f for the three types of the proposed springs.

Based on the obtained results in Figure 8 and Figure 9, it was found that a proportional relationship is noticed between t and z-mode oscillation frequency for the spring types. The operating frequency range is different for the three types, as follows:

- Type A: ranges between (50 and 375) kHz.
- Type B: ranges between (50 and 310) kHz.
- Type C: ranges between (50 and 310) kHz.

Then, the behaviour of all the different spring types will be examined as the length of the spring's inner boundary (L_{IB}) ranges between 2 μm and 20 μm, while all other parameters have not changed. The simulation findings, provided in Figure 10 and Figure 11, indicate that the increase in (L_{IB}) leads to increase the spring's circular arc length, and decreasing the oscillation frequency of the studied spring types. Also, the z-mode frequency alteration range is as follows for the three different types.

- Type A is around 600 kHz.
- Type B is around 550 kHz.
- Type C is around 550 kHz.

The operation frequency values of both type B and C remains the same. However, a separation is included in their 2nd oscillation mode, as shown in Figure 10b. The relative frequency change (δ_f) of type A is greater than 60% and increases to reach 78% as L_{IB} starts at 2 μm to reach 20 μm. The contrary was for the δ_f values for Type B and Type C, in which they decrease with increasing the L_{IB} value. Additionally, they are always less than the values of type A.

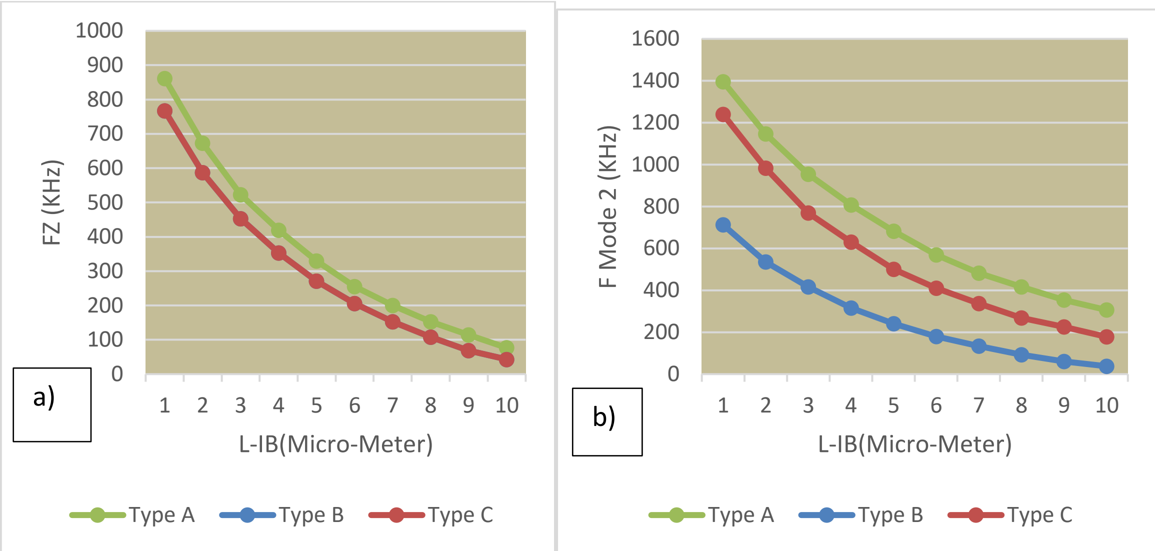

Figure 10: (a) z-Mode frequency, (b) mode 2 frequency.

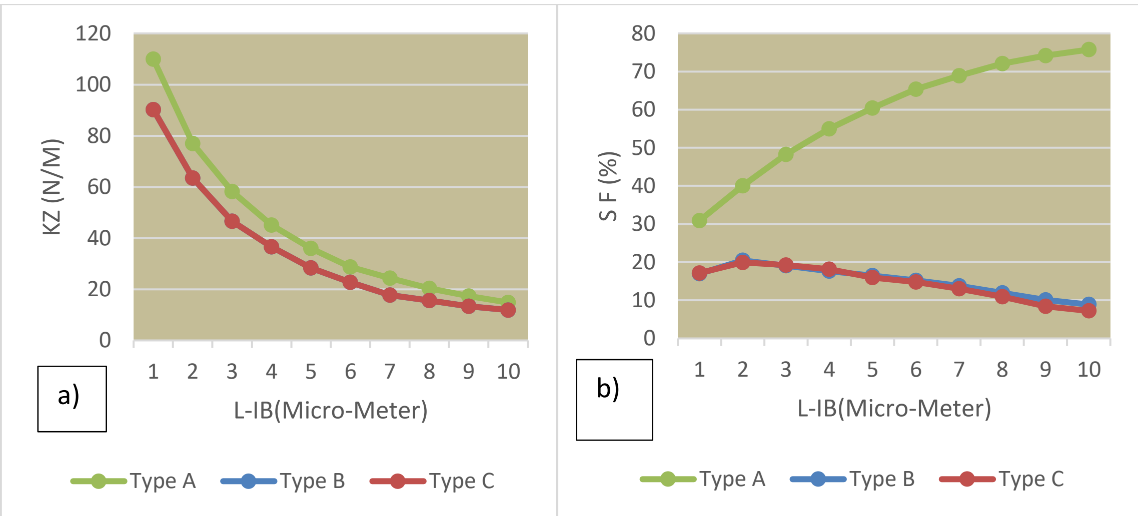

Figure 11: (a) mode z stiffness (b) δ_f for the three types of the proposed springs as a function of L_{IB}.

In the last stage of the study, the researchers examined the performance of three different types of springs when the coupling length (L_{IS}) was varied between 2-20 micrometres. The simulation results are provided in Figure 12 and Figure 13. The findings indicate that the operating frequencies of the three studied types of springs increase proportionally with a relatively small range of change of around 50 kHz. Additionally, the (Type B and Type C) operating frequencies are the same. Furthermore, the Type A spring, however, has a

delta f value greater than 75% that increases regularly to reach 85% as the L_{IS} increases between 2 micrometers and 20 micrometers. Otherwise, the increase in L_{IS} leads to decrease the delta f value for Type B and Type C.
Hence, the obtained results from Figure 6 through Figure 13 showed that Type A spring has δ_f that is superior compared with the rest types. Furthermore, the behaviour of Type C and Type B is not altered depending on the springs arrangement. Hence, when coupling bars within a single serpentine spring is used in the plane, the resistance of Type A is increased while the set operating frequency is the same of Type B and Type C.

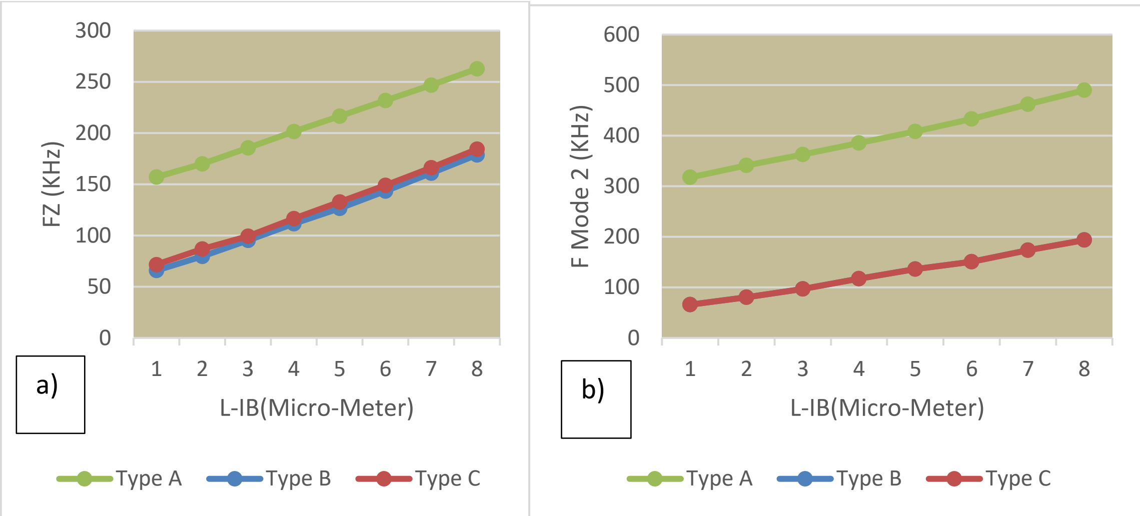

Figure 12: (a) Mode z frequency, (b) mode 2 frequency.

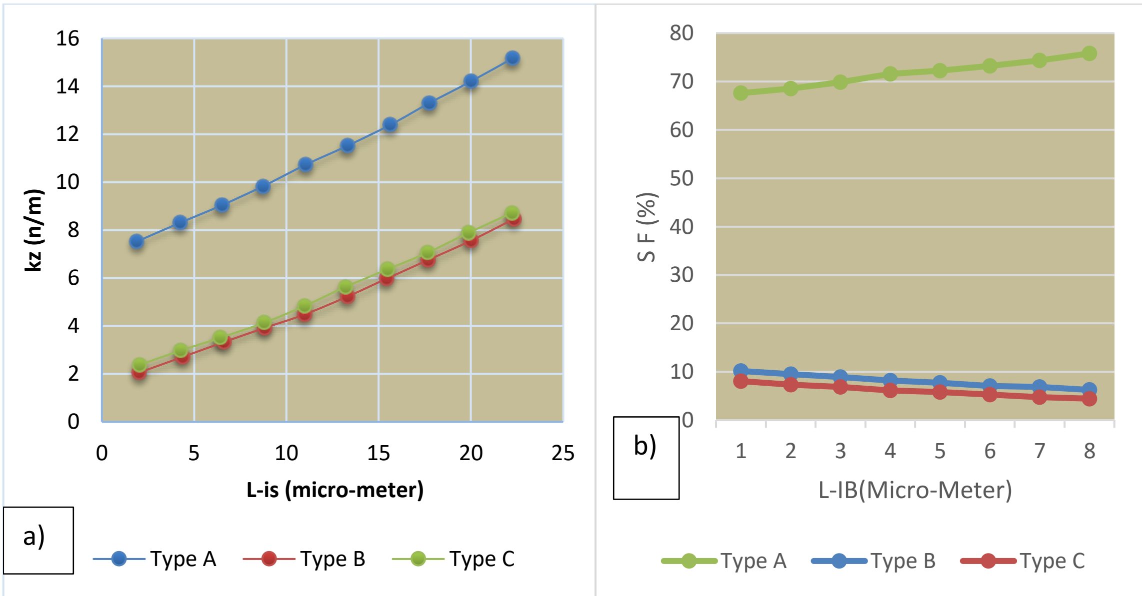

Figure 13: (a) mode z stiffness (b) δ_f for the three studied types of the proposed springs as a function of L_{IS}.

B. Comparison

In the previous section, the simulation outcome of the three studied types of spring were shown, with Type A displaying more efficient characteristics when compared to the other types (Types B and Type C). Additionally, the Type B performance was found to be like Type C performance.
In this section, the computational models will be used for designing micro-actuators using spring types A, B, and C. To make it easier to compare the different models, we will use the following symbols to represent them:
The variance among the two gathered natural frequencies, which are the calculated frequency (f_c) and the FEM natural frequency (f_m), depending on three different calculation methods (method-1, method-2, and method-3) is represented by (Δf 1-A), (Δf 2-A), as well as (Δf 3-A), regarding Type A, On the other hand,

(Δf 1-B) and (Δf 3-B) represents the variance between f_m and f_c based on (method-1 and method-2) regarding Type B. Accordingly, the variance between fm and fc can be evaluated using the following formula:

$$\Delta f\ i - A(B)\ =\ (f_c - f_m)/\ f_m\ \times\ 100\%$$

Next, we will examine the scenarios of changes in the spring's dimensional parameters, as investigated through FEM previously. A comparison between the calculated results by the models and the results obtained by FEM.

Figure 10 shows Δf errors in the numerical and analytical results. Figure 10 part (a) provides that regarding the beam width, the error ranges from 2 to 6 µm, which is greater than 20%. On the other hand, between 8 and 20 μm, the resulted error was lower than 10%. Whereas when the width of the beam is altered, the Sigitta model aligns with the interconnected springs' structure, while the model for straight beams and springs is appropriate for the independent springs structures.

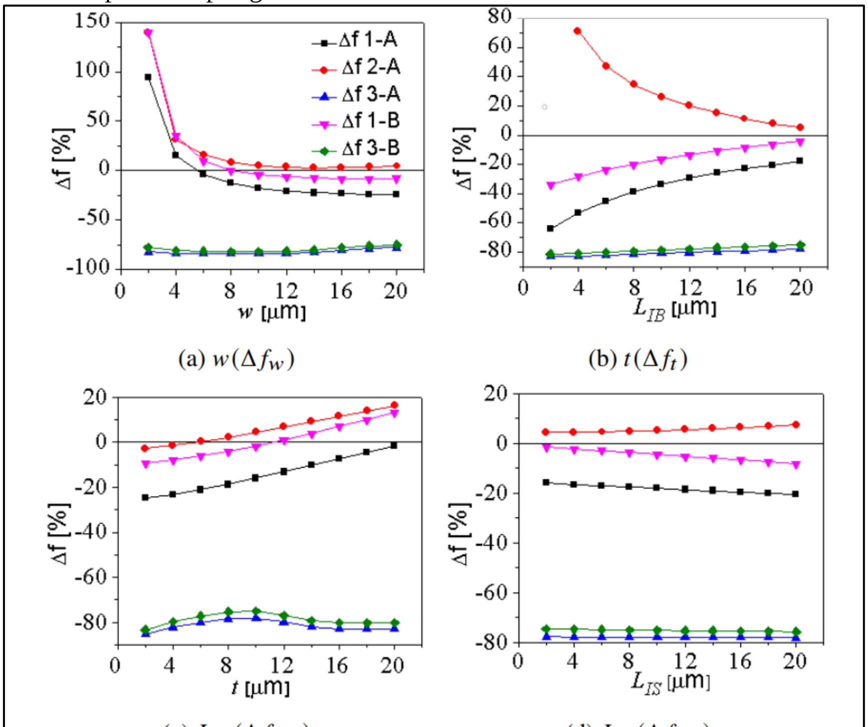

Figure 14: Comparing the outcome of calculating the natural frequency by utilizing the theoretical models outlined in Section 2 with the previous numerical methods based on the springs' dimensions.

The study's results compare the accuracy of two models for simulating the behaviour of springs: In the case of the coupled spring structure, the most suitable model to be used is the Sigitta model, whereas in the case of the uncoupled spring, the most suitable model is the straight beam spring model. The study found that when the thickness of the beam changes, the calculation error using the Sigitta model is less than 15% compared to the straight beam spring model, as shown in Figure 10 part (b). The difference between the two models ranges from 5-25%.

The study also found that as the length of the interconnection between the beams changes from 2 to 10 micrometres, the difference in the results (Delta f) is greater than 20%, as shown in Figure 10 part (c). However, as the length increases from 14 to 20 micrometres, the (Delta f) decreases to less than 10%. Lastly, the study found that the change in the coupling length between the spring's changes, the variation between the straight beam spring model, as well as Sigitta model is lower than 10%, and the Delta f values utilising the straight beam spring model in both uncoupled and coupled spring are more than 15%.

The comparison in the previous research released that the Sigitta model is appropriate for simulating the behaviour of coupled springs, whereas the model of the straight beam spring is better suited for simulating uncoupled springs. Both models demonstrated low calculation errors (less than 10%) when the width of the beam was between 8-20 micrometres, the thickness of the beam between 2-20 micrometres, the length of the connection between circular spring arcs varied between 12-20 micrometres, and the length of the coupling between two serpentine springs was varied between 2-20 micrometres. This is likely because the model of the straight beam spring does not consider the coupling between serpentine springs, whereas the Sigitta model considers this effect. Additionally, the Sigitta model also accounts for the angular deflection, which is denoted by (α) of the spring beams as shown in Figure 4 part (c), which makes it more appropriate for simulating the spring structure than the approximate straight beam spring model.

CONCLUSION

In this study, a model for a coupled spring system has been developed that focuses on reducing out-of-plane oscillation though suppressing other oscillation modes. This model has been shown to be more effective than similar spring systems that do not have coupling among the spring beams components. Furthermore, the coupling spring system has a greater variance between its operational frequency and several adjacent modes, which is larger than 60%. Additionally, this system has a wide range of operational frequencies, from 70 kHz to 900 kHz. Furthermore, in this work, methods for estimating the spring system's natural frequency have been developed, and it was found that the Sigitta spring model is appropriate to be used with the coupled spring structure, although the model of straight beam spring is appropriate for the uncoupled spring structure.

REFERENCES

Buśkiewicz, J., 2022. 1 Kinematic synthesis of the mechanism for static balancing of an input torque in three positions. *Archive of Mechanical Engineering,* 4(69), pp. 571-594.

Calmé, B., Rubbert, L. & Haddab, Y., 2022. Towards a Discrete Snake-Like Robot Based on SMA-Actuated Tristable Modules for Follow the Leader Control Strategy. . *IEEE Robotics and Automation Letters,* 8(1), pp. 384-391.

Dimian, A. & Bildea, C., 2014. Integrated design and simulation of chemical processes. *Elsevier.*

Guo, S. et al., 2022. Elastic energy storage technology using spiral spring devices and its applications: A review. *Energy and Built Environment.*

Hibbeler, R. C., 1994. *Mechanics of materials.* . s.l.:MacMillan Publishing Company. Journal of Micromechanics and Microengineering, 22(9).

Hu, F., Li, Z. & Qian, Y., 2012. A multi-electrode and pre-deformed bilayer spring structure electrostatic attractive MEMS actuator with large stroke at low actuation voltage. *Journal of Micromechanics and Microengineering,* 22(9).

Hu, X. X. et al., 2021. Improved resolution and cost performance of low-cost MEMS seismic sensor through parallel acquisition. *Sensors*, 23(21), p. 7970.

Jangra, M., Arya, D. & Khosla, R., 2021. Maskless lithography: an approach to SU-8 based sensitive and high-g Z-axis polymer MEMS acceleromete.

Larkin, K., 2020. Nonlinear Size Dependent Analysis and Crack Network Modeling of Micro/Nano-systems. *Doctoral dissertation, New Mexico State University.*

Liu, M., Wu, X. & Niu, Y., 2022. Research Progress of MEMS Inertial Switches.

Mouro, J., Pinto, R., Paoletti, P. & Tiribilli, B., 2020. Microcantilever: Dynamical response for mass sensing and fluid characterization. *Sensors,* 21(1), p. 115.

Muscat, A., Bhattacharya, S. & Zhu, Y., 2022. Electromagnetic vibrational energy harvesters: a review. *Sensors*, 22(15), p. 5555.

Rao, K. et al., 2019. A MEMS micro-g capacitive accelerometer based on through-silicon-wafer-etching process. *Micromachines*, 10(6), p. 380.

Singh, N., 2013. General review of mechanical springs used in automobiles suspension system. *Int. J. Adv. Engg. Res. Studies/III/I/Oct.-Dec*, pp. 115, 122.

Tu, X., Song, G. & Chen, Z., 2019. State of the art and perspectives on silicon photonic switches.

Wai-Chi, W., Azid, A. & Majlis, B., 2010. Formulation of stiffness constant and effective mass for a folded beam. 62(5).

Zang, H., Zhang, X., Zhu, B. & Fatikow, S., 2019. Recent advances in non-contact force sensors used for micro/nano manipulation. *Sensors and Actuators A: Physical*, Volume 296, pp. 155- 177.